Proceedings of MARTEC 2010
The International Conference on Marine Technology
11-12 December 2010, BUET, Dhaka, Bangladesh

COMPUTATIONAL STUDY ON THE FISH-LIKE UNDERWATER ROBOT WITH TWO UNDULATING SIDE FINS FOR VARIOUS ASPECT RATIOS, FIN ANGLES AND FREQUENCIES

Md. Mahbubar Rahman [1], Yasuyuki Toda[2] and Hiroshi Miki [3]

Department of Naval Architecture and Ocean Engineering, Graduate School of Engineering,
Osaka University, 2-1 Yamadaoka, Suita City, Osaka 565-0871, Japan.
[1]rahman@naoe.eng.osaka-u.ac.jp, [2]toda@naoe.eng.osaka-u.ac.jp, [3]Hiroshi_Miki@naoe.eng.osaka-u.ac.jp

ABSTRACT

The undulating fin propulsion system has been studied by many researchers including authors' group as a kind of bio-inspired propulsion system. In this study, the swimming motion of a Fish-like body with two undulating side fins similar to a Stingray and a Cuttlefish was investigated through flow computation around the body. In CFD technique, the Finite Analytic Method for space discretization and Euler implicit scheme for time discretization were used along with the PISO algorithm for velocity pressure coupling. A body-fitted moving grid was generated numerically using the Poisson equation at each time step. The features of the flow field and hydrodynamic forces acting on the body and fin were discussed based on the computed results. A simple relationship among the fin's principle dimensions was established. To investigate this relationship, the numerical computation was conducted for various aspect ratios, fin angles and frequencies. The relationship was examined base on the distribution of pressure difference between upper and lower surface and the thrust force distribution. Finally, the computed fin open characteristics was compared with the experimental results of the authors' previous studies.

Keywords: Biomimetics, Fish robot, Undulating side fins, Hydrodynamics, Thrust force, Computational Fluid Dynamics (CFD).

1. INTRODUCTION

Natural selection is often believed to be the best possible selection because each species has its own unique and optimum way of interacting with its environment obtained through the evolutionary natural selection process that favored the best. Robotic engineers borrow the sense and structure from the animals of the nature to optimize their designs. This study was based on a fish-like robot that used the undulating side fin for propulsion. In the field of underwater robotic research, undulating-fin robot offers exceptional advantage over propeller in preserving an undisturbed condition of its surroundings for data acquisition. Though the movement of this biomimetic type of robot is slow, it has interesting areas of applications such as in covert operations, in experimentations where minimally disturbed surrounding is of prime importance.

Since the demand for high-efficiency underwater vehicle is increasing, many researchers are interested in studies in this field. Many new concepts of biologically inspired underwater propulsion system have been developed including several undulating-finned robots (Sfakiotakis et al., 1999 and Kato et al., 2004). Unfortunately, till date, the development of efficient and environmental friendly underwater vehicle with undulating side fins is not up to the mark and it offers adequate opportunity to contribute to this field.

In our laboratory, a fish like underwater robot with undulating side fins similar to Stingray and Cuttlefish has been studied for many years (Figure 1). The aim of the project was to develop an efficient and environment friendly underwater vehicle. To begin with, the computation of the flow field around the simple model with undulating fins and resistance body was presented (Toda *et al.,* 2002A). The feature of flow field and hydrodynamic forces acting on the body and fins was elucidated based on the computed results to augment the understanding of the complex fluid mechanics that fishes use to propel themselves. Preliminary experiments reported Model 1 with a strut operated at very low frequency (Toda *et al.*, 2002B). Next the experimental results using the second model (Model 2) were presented (Toda *et al.*, 2004). It was followed by report using Model 2

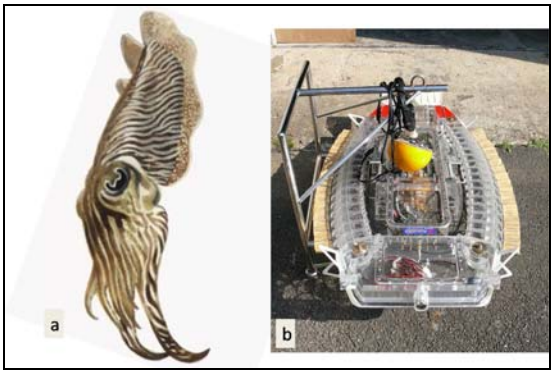

Figure 1. Photo of (a) Cuttlefish (b) Fish-like robot

consisted of 16 servomotors for both sides. The strut of model 1 and the big cables of Model 2 hindered their free movement for which in Model 3 was constructed without strut and big cable (Toda *et al.*, 2006). Model 3 had 17 servo motors for both sides to produce any fin's motion with the servo controller and the microcomputer being housed inside the model. Though Model 3 demonstrated the motion in the 6 degrees of freedom direction with greater control it had some limitations in adjustment of vertical gravity center and in communicating over a large distance. In order to overcome these discrepancies, Model 4 was constructed by using wireless LAN communication device and the gravity center adjustment system in three directions inside the model. The fin width was kept the same as the Model 3 but the fin length was increased a little resulting in a change in aspect ratio. Recently the preliminary experimental results demonstrated the ability of the new model (Toda *et al.* 2009). The simple prediction for different aspect ratios of fin was also shown and the new model shows improved performance than before.

The experimental and numerical studies are complementary to one another. Experiments can give the total force characteristics but for the detail analysis of force the numerical study is essential. So a numerical study was also conducted to recognize the flow physics around the undulating fin and to investigate the mechanism of thrust generation (Rahman *et al.*, 2010A). But that study was limited to one fin angle and few numbers of frequencies; the present paper discussed the similar phenomenon but for two fin angles and large number of frequencies. The objective of this study was to establish a simple relationship among the undulating side fin's principal particulars and hydrodynamic forces.

2. METHODOLOGY

The Model sketch and coordinate system is shown in Fig. 2. The body is symmetric with respect to x-axis, so only half of the body (shaded region) was simulated to save the computational effort. The width of the resistance body and the fin were denoted by b and b_m respectively. Also u, v and w were the velocity components for x, y and z directions respectively. Computation for the similar fin geometries used in the experiment has been conducted for comparisons. However, the resistance body was considered as flat plate and the sides were considered as straight for simplicity in the grid generation. At first, the numerical grid was constructed around a flat plate. Then two fins were produced at the lateral sides of the flat plate.

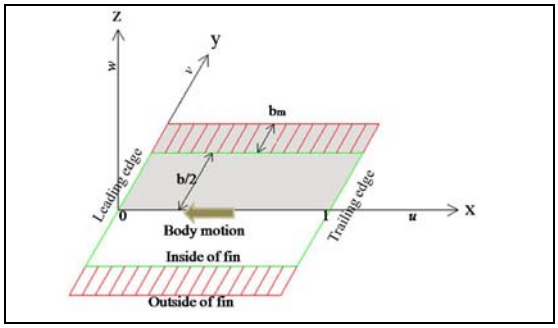

Figure 2. Simple model sketch and coordinate system

All variables were non-dimentionalized using resistance body length (L), advanced speed (U), density (ρ) and their combinations. The time history of fin angle in x-direction $\theta(x,t)$ was expressed in Eq. 1~2.

$$\theta = \theta_m \sin(2\pi nt - 2\pi x) \quad (1)$$

$$\theta_m = \arcsin\left[\left\{1 - 0.905\left(x - 0.5\right)^2\right\}\sin\Theta\right] \quad (2)$$

where,

θ : The deflection angle from flat plate ($0 < x < 1$)

θ_m: The angle amplitude ($0 < x < 1$)

n : Frequency (non-dimensional)

t : Time (non-dimensional)

x : Distance along fin from leading edge; and

Θ : Maximum fin angle from the flat position

A moving grid was constructed around the body to handle unsteady motion. A numerical grid was generated around half of the body at each time step using Poisson equation. At the first period the flat plate became fin by gradually increase its amplitude and other periods were symmetric. The grid independency was confirmed by checking different number of grids. The enlarged view near the fin of the grid is shown in Fig. 3. The body was covered by 41 and 16 grid points in x and y direction respectively.

Minimum grid spacing was 0.0015 non-dimensional lengths in the *y* and *z* direction.

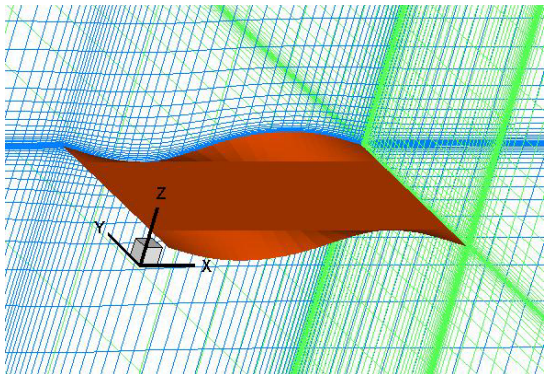

Figure 3. Computational grid near the fin

The computational domain and the number of grids for half domain are shown in Table 1.

Table 1. Computational domain and grid points for half domain

Axis	Computational domain	Number of grid points
x	-1 ~ 4	90
y	0 ~ 3	40
z	-3 ~ 3	51

The method of computation and boundary conditions were briefly discussed by Rahman (2010B). The Navier-Stokes equations and continuity equations were discretized by the 12- point Finite-Analytic method in space. Euler implicit scheme were used for time discretization along with the PISO algorithm for velocity pressure coupling. The laminar flow computation was carried out at Re = 10,000.

3. RESULTS AND DISCUSSION

3.1 Forces

For validation of the code, the computation was first conducted on the flat plate having similar area of the model. In the simulation, the velocity of the flow was gradually accelerated from 0 to 1 and then kept at steady state. The computational frictional force of flat plate agreed well with the well-known Blasius solution (B/L × 0.01328) in the steady state region (Figure 4).

The core aim of the thesis was to analyze the hydrodynamic forces produced by different fins. So the computation was conducted at different aspect ratios and fin angles for different frequencies. Sufficient convergence was ensured by taking adequate iteration in all the cases. The time history of x-directional forces at aspect ratio (b_m) of 0.1, frequency (n) of 4 and maximum fin angle of 30^0 was drawn (Fig. 5). The robot we used mimicked the flat fishes with undulating side fins which usually use the progressive wave based swimming mode. In this mode, to propel forward, the progressive wave

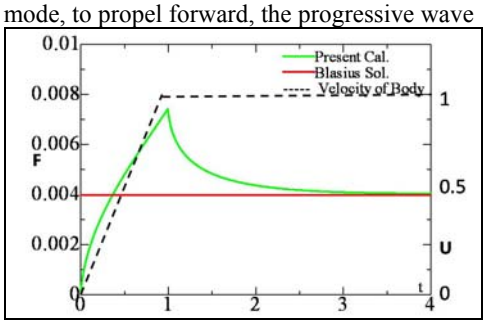

Figure 4. Frictional force for a flat plate in acceleration stage and constant velocity stage.

must be faster than the uniform flow. This is one kind of lift-based swimming mode, where no recovery stroke is necessary because lift force can be generated during the upstroke and downstroke of the fin.

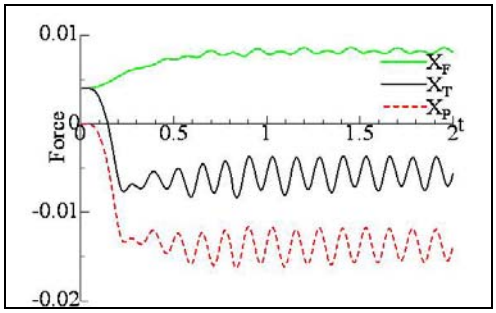

Figure 5. Time history of *x*-directional forces for AR = 0.1, n = 4 and $\Theta = 30^0$

In this fashion, *x*, *y* and z direction forces were produced during the movement of the undulating side fins (Fig. 6). The *z*-direction force is large but the body doesn't go up or down because of its flat shape; the mean of *z*-component force is zero. The *y*-component is also generally cancelled out due to the symmetrical movements of two side fins. So, only the *x*-direction force acts on the body. In this figure, it is also observed that, the *x*-component

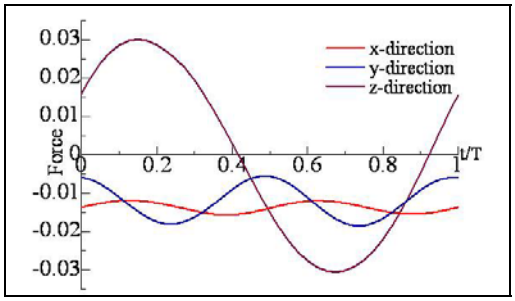

Figure 6. *x*, *y* and *z* direction pressure forces produced by undulating side fin.

force shows two peaks in one period which indicated that the fin produced force in both

upstroke and downstroke movements. The total forces for one period of aspect ratio 0.1 at different frequencies and maximum fin angles are shown in Fig. 7. From this figure, it is mentionable that for maximum fin angle of $\Theta = 30^0$ and $n = 3$ the total force is very near to zero. This is in agreement with the experiment as the self propulsion frequency of the model was similar to this value.

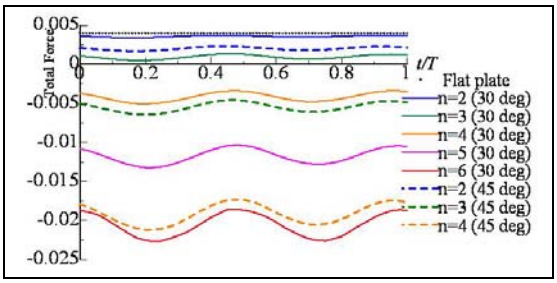

Figure 7. Time history (one period) of the *x*-directional total force for AR = 0.1 at different frequencies and maximum fin angles.

The amount of thrust and the propulsive efficiency depend mostly upon the aspect ratio and fin angle. High aspect ratio fins are more efficient as they induce less drag per unit of lift or thrust produced.

3.2 Contours

Different contours were drawn to visualize the surface distribution of forces and velocities.

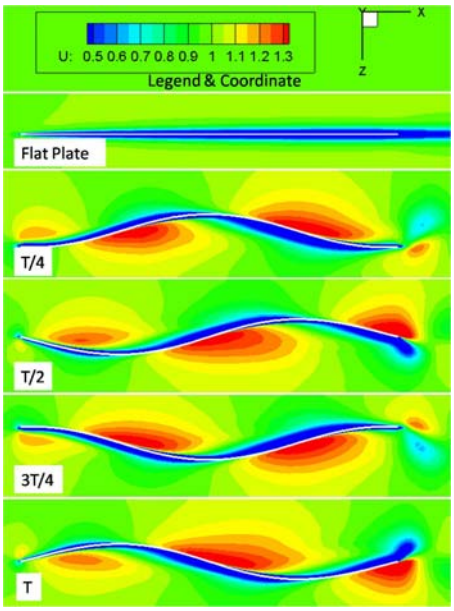

Figure 8. *u*-velocity distribution on a flat plate and around a fin (AR = 0.1) for *n* = 4 at four time steps in one period

The contour of *x*-directional velocity distribution on a flat plate, is shown in Figure 8. The figure shows the boundary layer very clearly around the flat plate. It also shows the *x*-directional velocity distribution around the undulating side fins at different time steps in one period. From the figure, the velocity gradients at different positions of the fin are clearly visible.

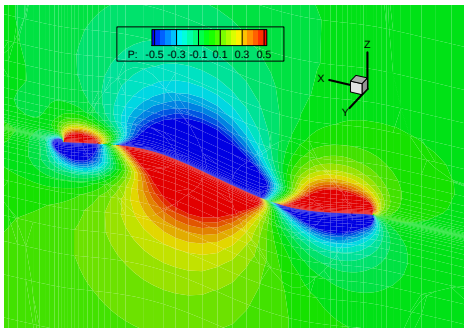

Figure 9. Pressure distribution on the upper and lower surfaces of the fin at *y* = 0.275

When the fin pushed the surrounding water during its movement, the velocity increased in that region. The fin's undulations reduced the boundary layer, resulting in increased velocity gradient and, hence, shear stress. The pressure difference between upper and lower surface during the fin's undulations is shown in Fig.9. The prediction of pressure difference between two surfaces is important because it is the main reason behind the thrust force generation.

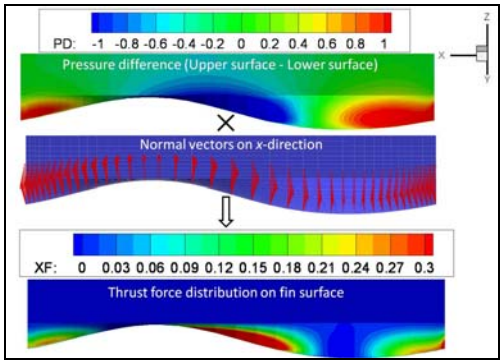

Figure 10. The method of thrust calculation

The thrust was computed by the product of pressure difference between upper and lower surface with the normal vectors to *x* (Fig. 10). The pressure difference distribution and the thrust distribution on the body and the fin at four time steps of one period is shown in Fig. 11. Two important phenomena should be discussed using this figure. Firstly, both for the negative and the positive pressure differences, the x-direction forces have maximum value. This confirmed the previous discussion of Fig. 6, which showed that the fin produces thrust during both of its upstroke and downstroke movements. Secondly, there is also

pressure difference on the body part, but the body cannot produce thrust force because the normal vectors are zero here.

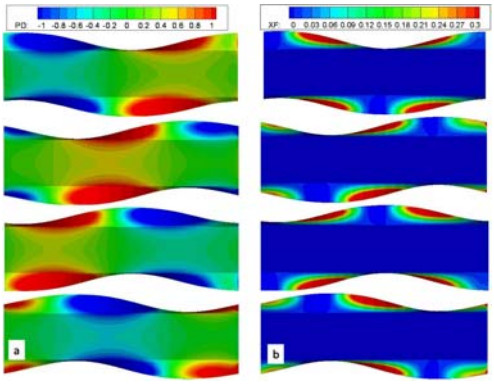

Figure 11. (a) Distribution of pressure difference ($p_{upper} - p_{lower}$); (b) Distribution of *x*-directional thrust force on the full body of AR = 0.1, *n* = 4 and $\theta = 30^0$ at four time steps in one period

4. FIN OPEN CHARACTERISTICS

4.1 Computed Result

The hydrodynamic force produced by the undulating side fins was computed to examine the relation between the thrust coefficient (K_x) and advance coefficient (J), similarly as in propeller chart. The thrust force (T_x) was estimated by subtracting the flat plate resistance from the total *x*-directional force in the similar manner as the experiment.

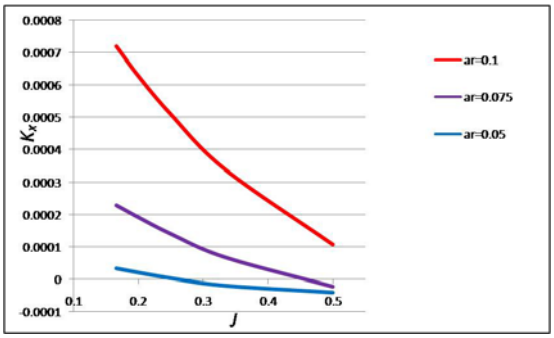

Figure 12. Fin open characteristics, $\Theta = 30^0$

The results for the force in axial direction (*x*-force) and advanced coefficient were computed in following non-dimensional procedure.

$$K_x = \frac{T}{\rho n^2 L^4} = \frac{T}{\rho U^2 L^2} \times \frac{U^2}{n^2 L^2} = T_x \times J^2 \qquad (3)$$

$$J = \frac{1}{n} \quad \left(= \frac{U}{NL}\right) \qquad (4)$$

The fin open characteristics for maximum fin angle of 30^0 and 45^0 are shown for aspect ratios of 0.05, 0.075 and 0.1 in Figure 12 and Figure 13 respectively. Each graph apposed in the expected tendency with the change of aspect ratio and fin angle. It is also found that the thrust produced by fin at maximum angle of 45^0 is nearly twice compared to that of 30^0.

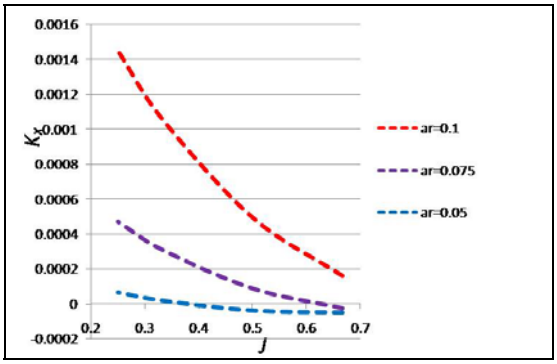

Figure 13. Fin open characteristics, $\Theta = 45^0$

4.2 Verification

The relation among thrust coefficient, aspect ratio and fin angle was derived as:

$$Kx = \Theta^2 \cdot \left(\frac{b_m}{L}\right)^3 \cdot \left(1 - \frac{U}{n\lambda}\right)^2 \cdot \int_0^1 \int_0^1 \left[4\pi^2 Cpb^2 \cos^2(2\pi k(s - ct))\right] \cdot dsdb \qquad (5)$$

From this equation is seen that the thrust coefficient is proportional to the cube of aspect ratio and square of maximum fin angle. These two relationships were established by the computation (Fig. 14). We know, (AR 0.1/AR 0.075)^3 = 2.37; so if we divide the AR 0.1 result by 2.37, it goes very near to 0.075's result. In the similar manner, as (Θ *45/* Θ*30*)^2 = 2.25, the thrust generated by fin at maximum fin angle of 45^0 is about 2.25 times of that at 30^0 irrespective of fin's aspect ratio.

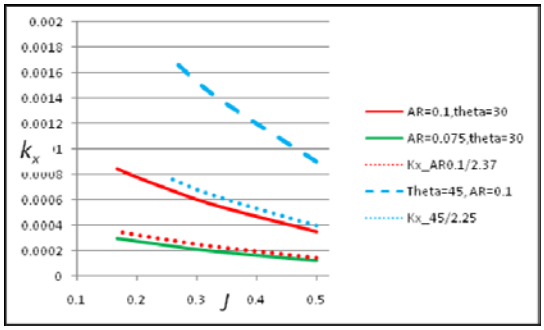

Fig. 14: The relation between k_x & AR and k_x & Θ

4.3 Comparison

The computed and calculated results were compared with the experimental ones. The experimental results for Model-3 and Model-4 with aspect ratios 0.136 and 0.09 are shown by blue and green dots, respectively (Fig. 15). The violet and the red lines show the computed results for AR 0.075 and 0.1. As the aspect

ratios of computed and experimental models were different, for more comparison the results for AR similar to the experiments was calculated using the

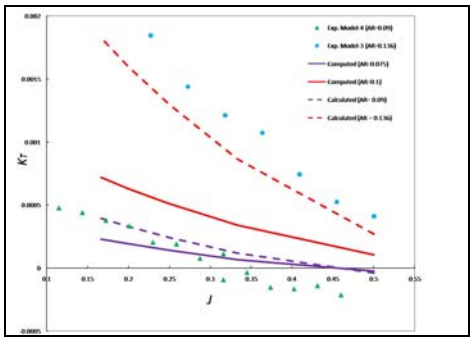

Figure 15. Comparison among the computed, calculated and experimental results, $\Theta = 30^0$

previous formula, which is shown by red and violet dash lines. The calculated result shows good agreement with the experimental result of corresponding aspect ratios. A little disparity is seen between the empirical and simulated results at first sight. But, this is due to the dissimilarities of the models.

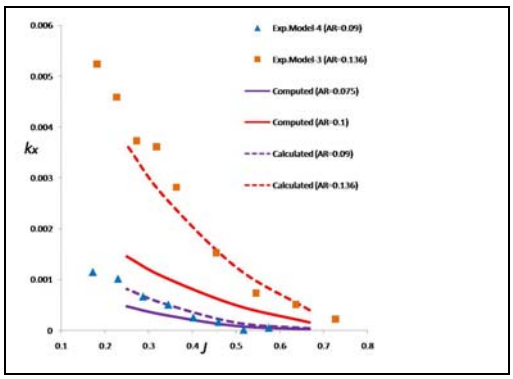

Fig. 16: Comparison among the computed, calculated and experimental results, $\Theta = 45^0$

The fin open characteristics for $\Theta = 45^0$ are also shown in Fig. 16. This result shows better conformity than the 30^0 results. This is because; the same area of the fin can make more pressure force when the maximum fin angle is increased. This is also consistent with the previous discussion. Over all, it is mentionable that, the computed result approached the expected trend with the changes of the aspect ratio and maximum fin angle.

5. CONCLUSION

The swimming motion of a fish-like body with two undulating side fins was investigated through flow computation around the body. The relationship between the relative velocity of fluid and the fin's surface were investigated based on the distribution of pressure difference of upper and lower surfaces and thrust force distribution. The computational model exhibited a considerable agreement with the empirical observations. A simple relationship among the fin's principle particulars and hydrodynamics was established using the computed result. The comparison between the force measurement and integrated force using CFD result for simple model showed that the CFD techniques can predict the hydrodynamic force produced by the undulating fin.

REFERRENCES

[1] Kato, N., Ayers, J. and Morikawa, H., "Bio-mechanism of Swimming and Flying," *Springer-Verlag,* Tokyo, Japan (2004).

[2] Rahman, M. M., Toda, Y. and Miki, H., "Study on the Performance of the Undulating Side Fins with various Aspect Ratios using Computed Flow, Pressure Field and Hydrodynamic Forces," *Proc. of the 5th Asia-Pasific Workshop on Marine Hydr.*, Osaka, Japan (2010A).

[3] Rahman, M. M., "Flow Computation Around Fish-like Robot with Undulating Side Fins," *M.Sc Thesis*, Graduate School of Eng. Osaka University, Japan (2010B).

[4] Sfakiotakis, M., Lane, D.M. and Davies J.B.C., "Review of Fish Swimming Modes for Aquatic Locomotion," *IEEE Journal of Oceanic Engineering*, vol. 24, No. 2 (1999).

[5] Toda, Y., Hieda, S. and Sugiguchi, T., "Laminar Flow Computation around a Plate with Two Undulating Side Fins*," Journal of Kansai Society of Naval Architects*, Japan, No.237 (2002A).

[6] Toda, Y., Fukui, K. and Sugiguchi, T., "Fundamental Study on Propulsion of a Fish-like Body with Two Undulating side Fins," *Proc. of The 1st Asia Pacific Workshop on Marine Hydrodynamics*, Kobe, Japan (2002B).

[7] Toda, Y., Suzuki, T., Uto, S. and Tanaka, N. "Fundamental Study of a Fishlike Body with Two Undulating Side-Fins," *Bio- Mech. of Swimming and Flying*, Springer, pp. 93-110 (2004).

[8] Toda, Y., Ikeda, H. and Sogihara, N., "The Motion of a Fish-Like Under-Water Vehicle with two Undulating Side Fins," *The Third Inter. Symposium on Aero Aqua Biomechanisms* , Ginowan, Okinawa, Japan (2006).

[9] Toda, Y., Danno, M., Sasajima, K and Miki, H., "Model Experiments on the Squid-Like Under-Water Vehicle with two Undulating Side Fins," *The 4th International Symposium on Aero Aqua Biomechanisms* , Shanghai, China (2009).